

pubs.acs.org/JAFC Article

# New Insights into pH-dependent Complex Formation between Lignosulfonates and Anthocyanins: Impact on Color and Oxidative **Stability**

Ana Rita Pereira, Carlo Bravo,\* Rui Miguel Ramos, Carina Costa, Alírio Rodrigues, Victor de Freitas, Nuno Mateus, Ricardo Dias, Susana Soares, and Joana Oliveira\*



Cite This: J. Agric. Food Chem. 2024, 72, 26820-26831



**ACCESS** I

III Metrics & More

Article Recommendations

Supporting Information

ABSTRACT: Anthocyanins have limited application as natural colorants and antioxidants due to their color loss and instability under certain conditions. This research explores the formation of a complex between lignosulfonates (LS) and cyanidin-3-Oglucoside (C3G) using a multitechnique approach as well as the effect on C3G's red color, oxidative stability, and antioxidant activity in acidic mediums. All data revealed pH-dependent LS-C3G interactions. The thermodynamic parameters showed weak noncovalent interactions, mainly electrostatic interactions, hydrogen bonds, and hydrophobic effect, with a higher association constant determined at pH 3. Fourier-transform infrared spectroscopy and Zeta-potential experiments further corroborate evidence of these LS-C3G interactions. Fluorescence quenching and lifetime experiments revealed static and dynamic quenching at pH 1 and 3, respectively. UV-visible spectroscopy demonstrated a bathochromic shift upon complex formation and a hyperchromic effect at pH 3 and 4, as a consequence of the improved red color of C3G. Electrochemical results suggested that at pH 3 the LS enhances C3G stability by protecting its oxidizable moieties over time, as well as improving the antioxidant activity of the anthocyanin in the complex.

KEYWORDS: hyperchromic effect, UV-visible, thermodynamic parameters, noncovalent interactions, fluorescence, redox

## 1. INTRODUCTION

Anthocyanins (ACNs) are biologically active phenolic compounds responsible for the orange, red, purple, and blue hues observed in different fruits, vegetables, and flowers.<sup>1,2</sup> Cyanidin-3-O-glucoside (C3G) is the most abundant ACN widely distributed in natural sources, especially in fruits such as blackberries, cherries, and red grapes.<sup>3</sup> These compounds are characterized by the flavylium cation or 2-phenylbenzopyrylium core structure, with variable methoxylation and hydroxylation patterns in the aromatic ring B. They can have sugar moieties connected to different positions, which confers good water solubility facilitating the incorporation of these dyes into food matrices. In addition to the food and beverage processing industry, ACNs find wide applications as colorants and antioxidant agents in cosmetics, textiles, and food packaging industries.<sup>4</sup> However, the stability of these natural compounds is affected by pH, temperature, oxygen, and light which limits their use as colorants due to color modification or color loss.<sup>5</sup> In addition, oxidation can lead to the deterioration and loss of the nutritional, commercial, and organoleptic quality.

Various strategies have been adopted to improve ACN stability by forming stable complexes with carbohydrates, proteins, and macrocycles. Hydrogen bonding and hydrophobic effects are the main driving forces for creating the complexes observed with carbohydrates and proteins, particularly in the presence of flavylium cation species.<sup>7,8</sup> Polysaccharides such as pectin have gained special attention as these compounds coexist in plant cell vacuoles and interact with ACNs, improving their bioavailability, extractability, and color stability, as these compounds can create a kind of nucleation site for anthocyanin adsorption, protecting the chromophore against water addition.  $^{9-11}$  Through hydrogen bonds, xanthan<sup>12</sup> and arabic gums<sup>13</sup> improved black rice ACNs color and thermal stability. Proteins, including  $\beta$ -lactoglobu- $\sin^{14}$  and milk  $\alpha$ - and  $\beta$ -casein,  $\sin^{15}$  have also shown potential to improve anthocyanin's photostability while preventing color fading and degradation. Macrocycles such as cyclodextrins incorporate ACNs inside their cavities, demonstrating higher affinity to the hemiketal, cis- and trans-chalcone forms of the anthocyanin multistate equilibrium, a phenomenon leading to the shifting of the pigment hydration equilibrium toward the formation of more colorless forms. 16,17

More recently, it has been reported the first evidence of the impact of commercial lignosulfonate on the thermodynamic and kinetic parameters of malvidin-3-O-glucoside at pH 1 using UV-visible spectroscopy.<sup>18</sup> Lignosulfonates (LS) are anionic polyelectrolyte polymers with an irregular threedimensional macromolecular structure, primarily composed

Received: July 1, 2024 October 31, 2024 Revised: Accepted: November 15, 2024 Published: November 21, 2024





of three phenylpropanoid units (*p*-coumaryl, coniferyl, and sinapyl alcohols). Due to the abundance of ionizable functional groups, including sulfonate groups, this lignin presents the advantage of being water-soluble. The skeletal lignin structure contains hydrophobic groups, consisting of aromatic and residual aliphatic units, and certain oxygencontaining groups. Their behavior in aqueous solution is largely determined by the proportion of hydrophilic (ionizable) and hydrophobic groups. Depending on the pH, LS can present different surface charges and conformations and interact with ACNs in various ways.

This work provides new insights into the red color stabilization and oxidative protection of C3G in the acidic pH range by a softwood lignosulfonate from the pulp and paper industry. The interaction between LS and C3G as well as the complex characteristics were achieved using a calorimetric and spectroscopic-based multitechnique approach namely, isothermal titration calorimetry (ITC), UV-visible and fluorescence spectroscopy, voltammetry, Fourier-transform infrared spectroscopy (FTIR) and electrophoretic light scattering (ELS).

## 2. MATERIALS AND METHODS

- **2.1. Reagents.** Lignosulfonates (average molecular weight of 48,566 g mol<sup>-1</sup>) were obtained from a softwood sulfite liquor (total solids, 11.3% w/w liquor), supplied by a pulp mill of a local company, as a mixture of 90% spruce (softwood material) and 10% beech (hardwood biomass). This liquor was submitted to an ultrafiltration process and the obtained retentate was freeze-dried to yield a goldenbrown powder. Specific conditions of this isolation process are described by Casimiro et al.<sup>21</sup> Hexadecyltrimethylammonium bromide (CTAB,  $\geq$ 98%) was purchased from Sigma. Commercial cyanidin-3-*O*-glucoside chloride was purchased from Extrasynthese ( $\geq$ 98%). Milli-Q water was used for the preparation of all solutions.
- **2.2. pH Determination.** The pH of all solutions was recorded (and if necessary adjusted using 1 M HCl or 1 M NaOH) in a WTW pH 320 or 508 (Weilheim, Germany) with a CRISON 5209 combined glass electrode of 3 mm diameter (Barcelona, Spain), previously calibrated with buffer solutions (pH 4.00, 7.00 and 10.00).
- **2.3.** Quantification of the Negative Groups in LS. The quantification of negative groups in the LS structure followed the established method described by Li et al.<sup>22</sup> LS (1 g L<sup>-1</sup>) and CTAB (0.01 M) stock solutions were prepared in Milli-Q water. Then, 10 mL of the LS solution was mixed with increasing volumes of the CTAB stock solution, ranging from 0.5 to 2.5 mL (in intervals of 0.1 mL), at each pH value (1 to 11). Water was then added to bring the total volume to 25 mL. Then, 1.5 mL of the resulting solution was centrifuged at 14,000 rpm for 10 min, and the absorbance of the supernatant was measured at 280 nm by UV–visible spectrophotometry using a 1 mm quartz cell. The number of negative groups, N (mmol g<sup>-1</sup>) was determined considering the CTAB volume corresponding to the minimum absorbance and following eq 1

Negative groups, N

$$= \frac{\text{CTAB volume(L)} \times \text{CTAB concentration(mol L}^{-1})}{\text{LS volume(L)} \times \text{LS concentration(g L}^{-1})}$$
(1)

**2.4.** Surface Charge of LS and the Complex LS-C3G. LS solutions  $(1 \mu M)$  were prepared in Milli-Q water across a pH range of 1–11, with the pH adjusted to the desired values using NaOH or HCl stock solutions. The solutions were filtered through a 0.22  $\mu$ m filter, allowed to equilibrate for 1 h, diluted 10-fold with deionized water adjusted to the desired pH, and transferred to a capillary cell. Stock solutions of C3G (100, 500, and 1000  $\mu$ M) were prepared in 0.1 M HCl for pH 1 experiences and in deionized water with pH adjustment for pH 3 studies. Solutions of the complex LS-C3G keeping the biopolymer concentration at 1  $\mu$ M and changing the concentration of

C3G (100, 500, and 1000  $\mu$ M) were also prepared in the same solvents of the stock solutions depending on the pH of the experiments. After 30 min of stabilization, the samples were transferred to the capillary cells, and the zeta potential values were determined. The average zeta ( $\zeta$ )-potential was measured by an Electrophoretic Light Scattering (ELS) using a Malvern Zetasizer Nano ZS instrument (Malvern Instruments Ltd., UK).

- 2.5. LS-C3G Interactions by Isothermal Titration Calorimetry. A MicroCal-PEAQ-ITC (Malvern Panalytical) controlled by MicroCal-PEAQ-ITC Analysis Software (version 1.41, Malvern Panalytical) was used to conduct isothermal titration calorimetry (ITC) experiments. Solutions of LS (150 μM) and C3G (5 mM) were prepared in a 10 mM citrate buffer for the experiments at pH 3 and 0.1 M HCl for the experiments at pH 1. Then, 240  $\mu$ L of the LS solution was loaded on the sample cell and the injection syringe was loaded with C3G solution. After reaching baseline stability, the C3G solution was injected (2 to 3  $\mu$ L/injection) into the sample cell 19– 22 times. Samples were stirred continuously at 1500 rpm to ensure full mixing. The time between injections (250-300 s) was optimized to allow reaching the baseline before subsequent injections. Raw data from a plot of heat flow vs injection number were fitted by the MicroCal-PEAQ-ITC Analysis Software to find the binding constants, stoichiometry, and thermodynamic parameters for the LS-C3G interactions studied using the one-site binding model. Blank experiments of C3G titration into 0.1 M HCl and 10 mM citrate buffer were performed and were subtracted from sample experiments.
- **2.6. Fourier-Transform Infrared Spectroscopy.** The Fourier-transform infrared (FTIR) spectra were recorded with an FTIR Spectrum (PerkinElmer) spectrometer equipped with a universal attenuated total reflectance (ATR) sampling device. Spectra were recorded in transmission mode over a wavenumber interval from 4000 to 600 cm<sup>-1</sup> (64 scans at a resolution of 2 cm<sup>-1</sup>). Analyses of the LS and LS-C3G complex were performed in a solid state after lyophilizing the solutions used in UV—vis experiments at pH 3.
- 2.7. Fluorescence Spectroscopy. Fluorescence quenching was measured using a Fluoromax-4 fluorimeter (Horiba Scientific). The emission spectra were recorded from 300 to 500 nm (scan rate 10 nm s<sup>-1</sup>) at two different excitation wavelengths (285 and 315 nmmaximum fluorescence peaks of LS). Both slit widths were set to 5 nm. The experiments were performed at pH 1 and 3 using 0.1 M HCl and 10 mM citrate buffer as solvents, respectively. The LS concentration was kept constant (0.82  $\mu$ M), while the concentration of C3G varied between 0-4.25 µM. The final concentrations of LS and C3G were optimized to guarantee adequate fluorescence intensity values while avoiding inner filter effects (UV absorbance at 285 and 315 nm under 0.1). 23 Absorbance measurements are summarized in Supporting Information, (Figure S1). The stock solutions were filtered (0.22  $\mu$ m filter) and maintained at 20 °C in a thermoshaker at 200 rpm (MSC-100 Cooling Thermoshaker Incubator) protected from light. The quenching mechanism was described by the Stern-Volmer eq (eq 2)

$$\frac{F_0}{F} = 1 + k_q \tau_0[Q] = 1 + K_{SV}[Q] \tag{2}$$

where  $F_0$  and F are the fluorescence intensities of LS before and after the addition of the quencher (C3G), respectively;  $k_{\rm q}$  is the bimolecular quenching constant;  $\tau_0$  is the lifetime of LS fluorophore; [Q] is the C3G concentration;  $K_{\rm SV}$  is the Stern–Volmer quenching constant.

In the 3D excitation—emission matrix (EEM) measurements, emission spectra (300—550 nm) were recorded at 2 nm increments of excitation wavelength between 250—350 nm at a scan rate of 20 nm s<sup>-1</sup>. The EEMs parallel factor analysis (PARAFAC) was used to quantify the effects of C3G on the LS fluorescence individual components and was conducted using the drEEM toolbox (https://dreem.openfluor.org/) in MATLAB. More details of the EEM-PARAFAC analysis are described in Text S1 and illustrated in Figure S2.

Time-resolved fluorescence measurements were performed with a TemPro 01 system (Horiba Jobin Yvon, USA). The samples were excited at 290 nm (NanoLED light source) and the emission was set to 376 nm (bandpass of 16 nm). Time-resolved experiments were recorded using a window of 4024 channels (time calibration of 0.055 ns/channel). To optimize the S/N ratio, 10,000 photon counts were collected at the peak channel.

2.8. Multistate of C3G Species by UV-visible Spectroscopy. The pseudoequilibrium and equilibrium constants for C3G were determined by UV-visible spectroscopy using aqueous solutions ranging from pH 0 to 6. A stock solution of C3G (2.6 mM) was prepared in 0.1 M HCl, and different stock solutions of LS (90  $\mu$ M) were prepared in water at pH values ranging from 0 to 6 with a pH tolerance of  $\pm 0.2$ . For pH 0, the stock solution of C3G was prepared in 1 M HCl. In each experiment, 981  $\mu$ L of water at the desired pH, 500  $\mu$ L of the LS solution (previously filtered with a 0.22  $\mu$ m filter), and 19  $\mu$ L of C3G stock solution were added into a plastic cuvette (10 × 10 mm). A control experiment without LS was performed by replacing the volume of LS with water. The absorption spectra of all solutions from 200 to 800 nm were recorded in a Cary 60 UV-visible spectrophotometer (Agilent) after 30 min (pseudoequilibrium, p $K_a$ ) and 1 day (equilibrium,  $pK'_a$ ). The fittings for the  $pK_a$  and  $pK'_a$  were carried out using the Solver tool in Microsoft Excel.

2.9. UV-visible Titration Experiments for LS-C3G Complex. The association constants between C3G and LS were determined at pH 1, 3, and 4 using UV-visible spectroscopy. For pH 1, the experiment was performed using 0.1 M HCl as the solvent, while for pH 3 and 4, Milli-Q water with pH adjusted with HCl (12 M) was used. Two solutions were prepared for each pH value: solution A containing C3G (26  $\mu$ M) and solution B containing C3G (26  $\mu$ M) and LS (30  $\mu$ M). Small volumes of solution B were then added to solution A to obtain solutions with increasing concentrations of LS (from 0.30 to 24  $\mu$ M). The absorption spectrum from 350 to 700 nm was recorded for all solutions in a quartz cell (10  $\times$  10 mm). The values of the apparent association constants (nK<sub>a</sub>) were determined using the Solver tool in Microsoft Excel, by fitting the obtained data from the graphical representation of the maximum absorption wavelength as a function of LS concentration. It used a mathematical model that considers the average number of binding sites in LS (n)available to interact with C3G and the concentration of LS ([LS]) in each point. 18 In this model, it was considered that the concentration of docking sites in the lignosulfonate is much higher than the concentration of complexed anthocyanin. The equation obtained to describe this interaction is eq 3

$$Abs = Abs_0 + \Delta Abs \frac{nK[LS]}{(1 + nK[LS])}$$
(3)

where Abs represents the absorbance,  $Abs_0$  is the initial absorbance,  $\Delta Abs$  is the change in absorbance, n is the number of functional groups in LS available for interaction, K is the association constant.

**2.10. Electrochemical Studies.** Square wave voltammograms (SWVs) were performed with a potentiostat driven (PalmSens4) by PSTrace software in a three-electrode cell consisting of a 3 mm glassy carbon working electrode (WE), an AglAgCl (3 M KCl) reference electrode and a Pt wire counter electrode (all from Basi, USA). The instrumental parameters used for the analysis were: square-wave frequency of 25 Hz, wave amplitude of 25 mV, and potential step of 5 mV (resulting in a scan rate of  $125 \text{ mV s}^{-1}$ ). After each measurement, the WE surface was renewed using 1.0  $\mu$ m aluminum oxide on polishing pads, thoroughly rinsed with Milli-Q water, and dried. The cleaning procedure was necessary to avoid underestimating anodic currents due to the passivation of the WE. SWVs were recorded at pH 1.0 (0.1 M HCl) and 3.0 (10 mM citrate buffer) in solutions containing: (i) only LS (1–20  $\mu$ M); (ii) only C3G (2–100  $\mu$ M); (iii) C3G with increasing concentrations of LS.

2.10.1. Antioxidant Activity – DPPH Assay. Standard DPPH assay was performed according to the literature, <sup>24</sup> with some modifications. In a 96-well plate, 270  $\mu$ L of DPPH solution (prepared in methanol at 60  $\mu$ M) was mixed with 30  $\mu$ L of the antioxidant sample. A range of concentrations was tested for C3G (1.03–20.63  $\mu$ M) and LS (0.21–10.30  $\mu$ M) to achieve the individual radical scavenging activity (RSA

%), monitored over time by measuring the DPPH absorbance band at 515 nm ( $\lambda_{\rm max}$ ) on a plate reader (Biotek Powerwave XS) at the beginning (t0) and after 20 min of reaction (t20). The RSA was calculated using the following equation: RSA (%) = (Abs Control-Abs sample)/(Abs Control) × 100, where Abs control and Abs sample are the absorbance of the Control at t=0 min and the tested sample at the incubation time, respectively. Three different concentrations of the LS-C3G complex were evaluated, based on individual RSA (%) values of C3G and LS, and keeping a 2.5 C3G-LS ratio. The antioxidant activity was also measured while keeping C3G at 2.6  $\mu$ M and increasing LS concentrations from 0.2 to 1  $\mu$ M.

**2.11. Statistical Analysis.** Analyses were performed in triplicates and the results were expressed as mean values and standard deviation (SD). All experiments were performed at room temperature, being that for fluorescence studies the temperature was controlled at 20  $^{\circ}$ C. Analysis of variance (ANOVA) was used to identify statistical significance, and differences were considered statistically significant at p < 0.05. GraphPad Prism 8.0 for Windows was used to process all statistical data.

## 3. RESULTS AND DISCUSSION

pubs.acs.org/JAFC

3.1. Characterization of LS in Aqueous Solution. The LS used in this work were isolated from a sulfite liquor and characterized based on inorganic content, phenolic monomers, <sup>13</sup>C NMR, and molecular weight, as detailed in Supporting Information (Table S1). Considering the hypothesis of electrostatic interactions between the positively charged C3G and the negatively charged groups of LS, the number of ionizable groups and the overall LS surface charge were investigated from acidic to alkaline conditions. LS comprises ionizable groups such as sulfonate, carboxylic, and hydroxyl groups. According to the literature, the degree of ionization of LS in aqueous systems is influenced by the pH, with sulfonate groups ionizing at pH 1.5, carboxylic groups at pH 5.1, and hydroxyl groups at pH 10.5.25,26 The zeta-potential revealed two inflection points: one at pH 4.2, attributed to carboxyl groups, and the other at pH 8.1 related to phenolic hydroxyl groups that may start to deprotonate, further increasing the negative charge on the surface (Figure S3a). Under acidic conditions (pH < 4), the zeta potential of LS decreased from −10 to −30 mV due to the successive ionization of sulfonic acid groups. Between pH 4 and 8-where the ionization of carboxylic groups occurs—the values of zeta potential remain constant, suggesting that these functional groups are not surface-exposed. At pH values higher than 8, the zeta potential became more negative due to the ionization of phenolic hydroxyl groups. These results suggested that both sulfonic and phenolic hydroxyl groups are distributed on the LS surface, while carboxyl groups are concentrated in the polymer's core. Deprotonated sulfonic acid groups can be directly involved in the interactions with C3G in the pH range studied (between pH 1 and 4).

The CTAB precipitation method was used to determine the amount of negative groups in LS. Since CTAB is a cationic surfactant that establishes an electrostatic interaction with the negative groups of LS, the amount of CTAB required reflects the content of negative groups in LS (Figure S4a). As the pH increases, a higher amount of CTAB is necessary to neutralize the negative charge of LS, indicating the presence of more negative groups (Figure S4b). Up to pH 4, the content of negative groups increased from 1.00 to 1.33 mmol g<sup>-1</sup> of LS due to the neutralization of the deprotonated sulfonic acid and carboxylic groups. Between pH 5 and pH 9, the results showed a plateau where the amount of negative groups was around

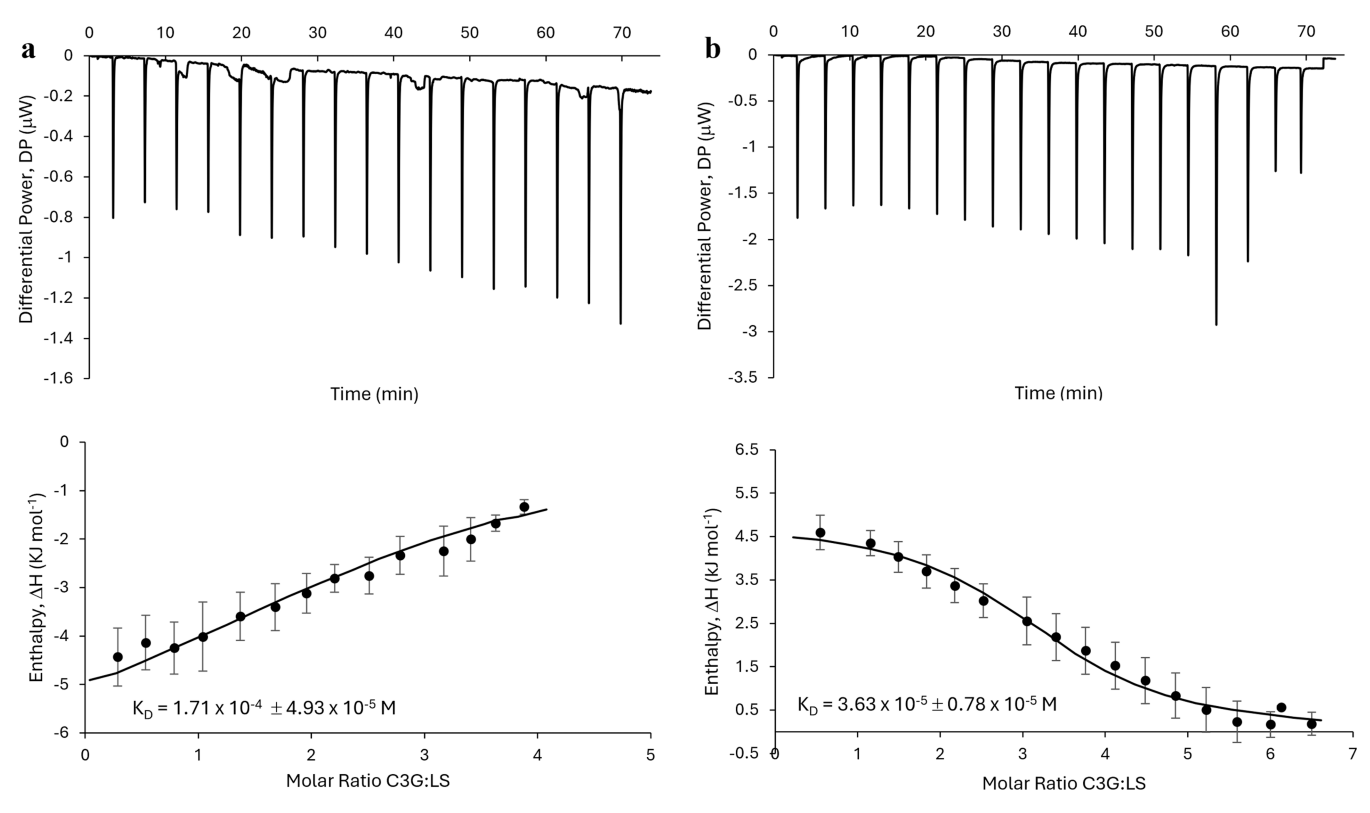


Figure 1. ITC isotherms for the LS (150 μM) with C3G (5 mM) at pH 1 (a) and pH 3 (b): binding isotherm (points) and fitting curve (line).

Table 1. Thermodynamic Parameters (Association Constants,  $K_a$ , Enthalpy,  $\Delta H$ , Gibbs Energy,  $\Delta G$ , and Entropy,  $-T\Delta S$ ) Determined for the LS-C3G Interaction<sup>a</sup>

pН	$K_{\rm a}~({ m M}^{-1})$	$\Delta G^{\circ}$ (kJ mol <sup>-1</sup> )	$\Delta H^{\circ}$ (kJ mol <sup>-1</sup> )	$-T\Delta S^{\circ}$ (kJ mol <sup>-1</sup> )
1.0	$0.61^{a} \times 10^{4} \pm 1.6 \times 10^{3}$	$-21.5^{\circ} \pm 0.1$	$-23.1^{e} \pm 2.6$	$0.61^{\rm g} \pm 0.04$
3.0	$2.8^{\rm b} \times 10^4 \pm 5.5 \times 10^3$	$-25.4^{\rm d} \pm 0.5$	$20.2^{\rm f} \pm 0.9$	$-45.6^{\rm h} \pm 0.8$

<sup>a</sup>Presented data were obtained by subtracting C3G titration into the buffer used for each experiment and results from at least three independent experiments. Data with different letters are statistically different (p < 0.05).

Figure 2. Network of chemical species of cyanidin-3-O-glucoside in acidic solutions.

1.53 mmol g $^{-1}$  of LS, which meant the ionization of the negative group reached equilibrium. At pH values higher than 9, the content undergoes a clear increase from 1.60 to 1.97 mmol g $^{-1}$  of LS (pH 12) due to the ionization of the phenolic hydroxyl groups. These results support the previously obtained zeta potential values: up to pH 5 and after pH 9 the ionization of sulfonic and phenolic hydroxyl groups occurs.

**3.2. LS-C3G Complex Formation.** *3.2.1. Thermodynamic Characterization of LS-C3G Interaction.* The binding affinity between LS and C3G was characterized by isothermal titration calorimetry (ITC). The enthalpy changes per mole of injectant (kcal/mol) were plotted against the molar ratio C3G/LS at pH 1 and 3 (Figure 1). The resulting binding isotherms were fitted by the MicroCal-PEAQ-ITC Analysis Software according to an independent site model. Due to their general shape (Figure 1),

it could be assumed that anthocyanins interact nonspecifically with lignosulfonates rather than binding to specific sites, as the binding isotherms do not exhibit the sigmoidal shape expected for a specific interaction. From these curves, the dissociation constants ( $K_{\rm D}$ ) were determined and indicated in the graphs. The association constants ( $K_{\rm a} = 1/K_{\rm D}$ ) and the thermodynamic parameters obtained from the analysis of the fitting of the ITC binding isotherms are summarized in Table 1.

The association constant  $(K_a)$  obtained by the ITC demonstrated a pH dependency, with the highest  $K_a$  value observed for the interaction between LS and C3G at pH 3  $(K_a = 2.8 \times 10^4 \,\mathrm{M}^{-1})$ . ACNs exhibit different forms in equilibrium depending on the pH of the medium. At strongly acidic conditions (pH  $\leq$  1), the flavylium cation (AH<sup>+</sup>) is the sole species, responsible for the red color of ACNs. As the pH

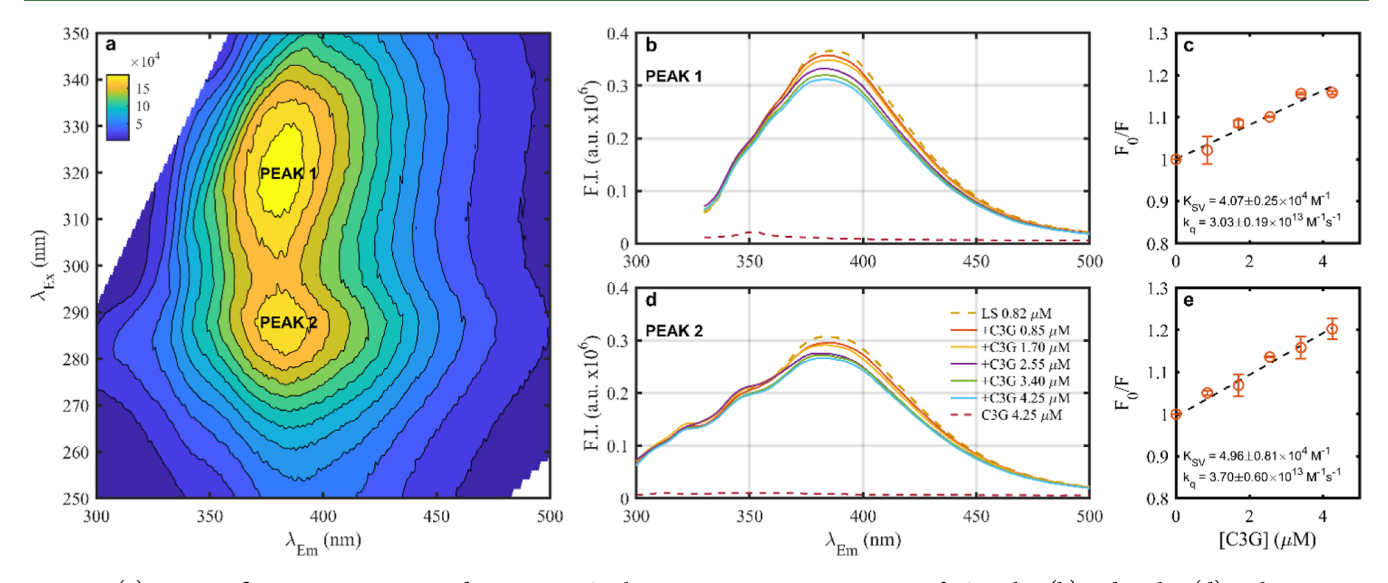


Figure 3. (a) 3D EEM fluorescence spectrum of a 0.82  $\mu$ M LS solution at pH 3. Emission spectra of LS Peak 1 (b) and Peak 2 (d) in the presence of increasing concentrations of C3G (0.42–4.25  $\mu$ M) and corresponding Stern–Volmer plots with the quenching and binding constants for C3G binding to LS (c,e). In plots b and d, the intrinsic fluorescence of C3G is reported as red dotted lines. The measured  $\tau_0$  value of 1.34 ns was considered for the calculation of the binding constant.

increases, the flavylium cation undergoes two simultaneous reactions: rapid deprotonation to generate the neutral quinoidal base (A, blue form), and a slower hydration process at carbon 2 resulting in the colorless hemiketal B (thermodynamically more stable than A). This form then undergoes ring opening (tautomerization) to produce cischalcone (Cc) which further isomerizes in trans-chalcone (Ct) (Figure 2).28 According to the data published by Leydet et al.,  $^{29}$  at 1.0 mM of C3G, the p $K_h$  should be approximately 3.5, which means that at slightly acidic conditions such as pH 3, 50% of anthocyanins are likely to occur as flavylium cation and the other 50% as neutral hemiketal form and quinoidal bases. Although electrostatic interaction is an important mechanism for the LS-C3G binding between the flavylium cation and the sulfonate groups of LS, the presence of other species can promote different types of interaction such as hydrophobic effects or  $\pi - \pi$  interactions between the aromatic rings of C3G and LS and explain the higher binding affinity at pH 3. Furthermore, the higher concentration of C3G used in the ITC experiments (5 mM) also induces self-association phenomena which limit the hydration reaction and favor the presence of flavylium cation in the solution available to interact with LS.<sup>29</sup> At very acidic conditions such as pH 1, flavylium cation is the only species in solution. This positively charged species can interact mainly by electrostatic forces with the negative groups of LS, which are the deprotonated groups in the structure of the polymer (p $K_a$  1.5). However, due to the presence of aromatic rings on the C3G and LS structures,  $\pi$ – $\pi$  stacking interactions and hydrophobic effects can also occur between the molecules, as observed in copigmentation between ACNs and flavonoids or hydroxycinnamic acids.<sup>30</sup>

The negative Gibbs free energy ( $\Delta G^{\circ}$  < 0) in both systems (Table 1) indicated that the interactions between LS and C3G are thermodynamically favorable, and the quite weak Gibbs energy observed for both pHs (-21 to -25 kJ mol<sup>-1</sup> at pH 1 and 3, respectively) suggested the presence of noncovalent interactions. Further thermodynamic analysis indicated that at pH 1 the LS-C3G interaction is exothermic (negative enthalpy,  $\Delta H^{\circ}$  < 0) driven primarily by enthalpy with negligible entropy

 $(\Delta S^{\circ})$  changes. Conversely, at pH 3, the interaction is endothermic ( $\Delta H^{\circ} > 0$ ) and entropy-driven (higher contribution for  $-T\Delta S^{\circ}$  parameter). In general, in systems with negative enthalpy  $(\Delta H)$  and positive entropy parameter  $(-T\Delta S)$ , as observed at pH 1, the interaction is essentially mediated by electrostatic forces and hydrogen bonds between ionized groups.31 At pH 3, the interaction is entropically driven, with a larger negative entropic parameter  $(-T\Delta S < 0)$ and a positive  $\Delta H$ , indicating that hydrophobic effects dominate this endothermic complex.<sup>32</sup> At this pH, neutral forms of C3G such as the hemiketal are in equilibrium with the flavylium cation and can create  $\pi$ -stacking interactions with macromolecules like LS, particularly in nonpolar or hydrophobic environments. However, the possibility of electrostatic interactions and hydrogen bonds between the ionizable groups of LS and the [AH+] form of C3G cannot be dismissed.

3.2.2. Surface Charge and Molecular Structure of LS in the Complex LS-C3G. The study of the surface charge of LS molecules corroborated the results observed in the thermodynamic parameters, suggesting a higher occurrence of electrostatic interactions at pH 1, which resulted in a significant variation in surface charge. Considering that these interactions primarily occur on the surface of molecules, particularly in the case of LS, which has been shown to have ionizable groups on the structure's periphery, the surface charge of LS was evaluated with various concentrations of anthocyanin (0-1 mM). Experiments were carried out at pH 1 and 3 as LS has variable surface charges because of the successive ionization of sulfonate groups as the pH of the medium increases. At pH 3, the zeta value of LS is more negative (around -30 mV) compared to the value for pH 1 (-19 mV), indicating more deprotonated functional groups (sulfonated groups). At both pHs, higher concentrations of C3G made the zeta potential less negative, which means that the negative groups are unavailable due to the interaction with the positive charges from the flavylium cation of the anthocyanin (Figure S3b). This modification was more evident at pH 1 corresponding to a variation of 83% for the highest concentration of C3G (1000  $\mu$ M), while for pH 3 the increase of the zeta potential was

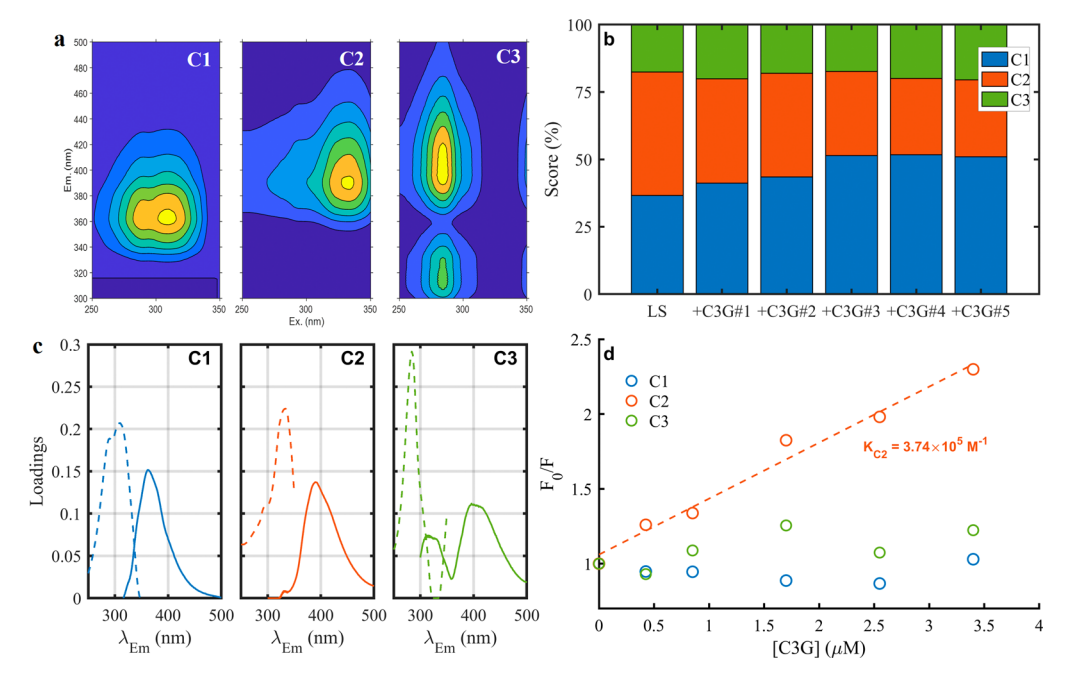


Figure 4. Fluorescence components detected in excitation—emission matrices and modeled by PARAFAC analysis of LS sample in the presence of increasing concentrations of C3G at pH 3 (a) and their relative score in each sample (b); (c) Excitation (dotted lines) and emission (continuous lines) loadings of each component; (d) Stern—Volmer plots of each component vs C3G concentrations.

around 41%. At pH 3, although the hydrophobic effect was the major mechanism for C3G-LS complex formation, the occurrence of electrostatic forces must be considered due to negative and positive charges in the solution that can interact and promote the complex formation. It was also detected that these modifications result from the electrostatic interactions between C3G and LS and not from a synergic effect by adding positive charges.

FTIR was used to perform complementary analysis on functional group modifications in LS molecules on the complex at pH 3. The data showed that the interactions with C3G resulted in some intensity variations in the aromatic region, without showing any shift in the peak positions. In agreement with literature data, 33-35 LS has characteristic wavenumber and corresponding vibration types (Table S2), since the most characteristic IR regions of LS are the C=C aromatic skeletal vibrations around 1500-1650 cm<sup>-1</sup>, and the sulfonic acid groups around 1150-1200 and 1030 cm<sup>-1</sup> (Figure S5). The intensity ratio between the peaks at 1600-1650 cm<sup>-1</sup> increased in the presence of C3G, suggesting that the aromatic rings of LS are the most prone to interact with the anthocyanin molecules through  $\pi - \pi$  interactions already mentioned in the ITC results. Furthermore, slight modifications on the band at 1200 cm<sup>-1</sup> characteristic of the sulfonate group (S=O) suggest possible interactions of this functional group with the C3G.

3.2.3. Fluorescence Evidence. The formation of the LS-C3G complex and the conformational changes of LS upon binding with C3G were followed by fluorescence. One of the intrinsic features of LS is its autofluorescence, attributed to fluorophores within the LS structure. While benzene rings, prevalent in all lignin monomers, largely contribute to fluorescence emissions, distinct side chains and substitutions on these rings can alter the emission spectrum, indicating the presence of multiple fluorescent structures within the lignin molecule.<sup>36</sup> To the best of our knowledge, this is the first study

investigating the quenching mechanism between LS and phenolic compounds. Similar studies only examined the binding mechanisms of LS with metal(oid)s, like Fe, Ag, and Hg. <sup>37,38</sup>

In all experiments, the chosen concentration of LS (0.82  $\mu$ M) was in the linear range of concentrations with fluorescence (Figure S6). The 3D EEM spectrum of LS at pH 3 (Figure 3 a) revealed the presence of two main peaks: peak 1 at  $\lambda_{\rm ex}/\lambda_{\rm em}$  of 315/385 nm, and peak 2 at a lower excitation wavelength ( $\lambda_{\rm ex}/\lambda_{\rm em}$  of 285/380 nm). The fluorescence quenching studies were performed for both peaks (Figure 3b-e). The interaction between LS and C3G was highly affected by the solution pH. Probably, because LS molecules are formed by different ionizable groups, the increase in the pH can promote the formation of negative charges responsible for electrostatic repulsion, which expands the molecule structure and favors the interaction with other molecules.<sup>39</sup> These modifications on the LS structure resulted in different fluorescence behaviors, since at pH 3, as seen in Figure 3c,e, was observed a linear Stern-Volmer equation, while at pH 1 a clear trend was not observed (Figure S7). Consequently, it was possible to only calculate the  $K_{sv}$  and  $k_{g}$ values at pH 3 (Figure 3e). The  $K_{SV}$  values found in this study were similar to those reported for C3G binding with proteins. 40-42 The higher values of the bimolecular quenching constant  $(k_q)$ , which could mean a quenching efficiency or fluorophores' accessibility to the quencher, compared to the diffusion-controlled limit  $(1.0 \times 10^{10} \text{ M}^{-1} \text{ s}^{-1})$  suggest an interaction.<sup>23</sup>

However, to understand the type of quenching involved in these interactions, time-resolved fluorescence experiments were performed using a similar approach to the one taken for steady-state fluorescence. The complex structure with random and disorganized linkages as well as branches makes the fluorescence lifetime of lignin very short in a range of subto nanoseconds. Furthermore, the fluorescence of LS is

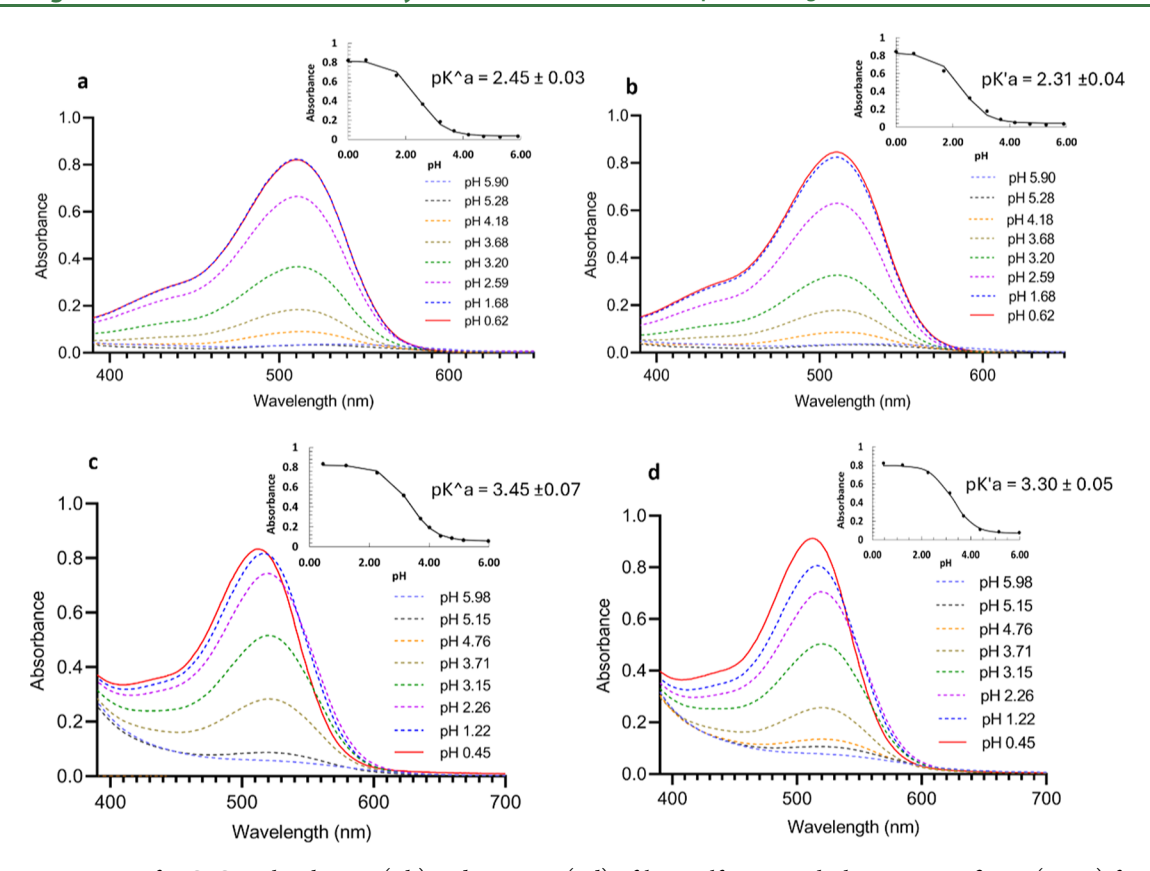


Figure 5. UV—vis spectra for C3G in the absence (a,b) and presence (c,d) of lignosulfonates with the respective fitting (insets) for the pseudo equilibrium (a,c) and equilibrium (b,d), respectively.

strongly dependent on the biomass nature and the applied pretreatment.<sup>43</sup> In agreement with the literature, <sup>44,45</sup> very small values for the lignin lifetime at both pH 1 and 3 were measured. While no significant changes in the fluorescence lifetime ( $\tau$ ) of LS were observed at pH 1 after the interaction of C3G, at pH 3 there was a slight decrease in the  $\tau$  value (Figure S8). These data can help to distinguish between static quenching at pH 1 and dynamic quenching at pH 3.

In static quenching, a nonfluorescent complex is formed, where the ratio of the fluorescence lifetimes in the absence and presence of the quencher ( $\tau_0/\tau$ ) equals 1, indicating that the fraction of noncomplexed fluorophores remains unperturbed. Electrostatic interactions suggested as the driving forces for the formation of the LS-C3G complex at pH 1 may promote the binding between the fluorophore and the quencher to form a nonfluorescent ground—state complex. On the other hand, collisions between the fluorophore and the quenching agent induce dynamic quenching, which is characterized by a decrease in the  $\tau$  of the excited state. <sup>23</sup>

All EEM spectra of LS samples at pH 1 and pH 3 measured in the absence and presence of C3G are shown in Supporting Information (Figures S9 and S10). Coherently with 2D results, the addition of C3G affected the fluorescence behavior of LS only at pH 3. Thus, only the EEM spectra at pH 3 were analyzed by PARAFAC (Figure 4). Split-half analysis, residual analysis, and visual inspection identified that three components were appropriate: C1 ( $\lambda_{\rm ex}/\lambda_{\rm em}$  310/360 nm), C2 ( $\lambda_{\rm ex}/\lambda_{\rm em}$  330/390 nm) and C3 ( $\lambda_{\rm ex}/\lambda_{\rm em}$  285/315–400 nm) (Figure 4c).

PARAFAC analysis provided additional quantitative information describing the distribution of the three components with increasing concentrations of C3G (Figure 4d), showing

that only component 2 was affected by the interaction with C3G. On the other hand, C1 and C3 did not show any significant decrease in intensity, highlighting the selectivity of the C3G interaction with LS.

3.3. Chromatic Characteristics of LS-C3G Complex. 3.3.1. Impact of LS on the Multistate of Species of C3G at Acidic Conditions. To evaluate the effect of LS in the multistate of species of C3G, C3G in the presence of LS was titrated across a pH range of 0 to 6 and the pseudoequilibrium  $(pK_a)$  and equilibrium  $(pK'_a)$  constants were determined. The UV-visible spectrum of each solution (C3G and C3G with LS) was recorded after 30 min (pseudoequilibrium) and 1 day (equilibrium) (Figure 5). This time scale allows for the establishment of equilibrium between AH+, B, and Cc forms at pH below  $\approx 5$ , and Ct formation over a longer period. Up to pH 6, there is a significant decrease in absorbance at 519 nm, corresponding to the disappearance of the AH<sup>+</sup> species to form B, Cc, and Ct. Acidity constants were determined from the graphical representation of the maximum absorbance (519 nm) as a function of the pH. As shown in Figure 5 (insets), the  $pK_a$  value closely aligned with  $pK'_a$  in the absence (Figure 5a,b) or presence of LS (Figure 5c,d) indicating that the contribution of the trans-chalcone form to the overall multistate species is below 10% in both cases. In the presence of LS, both acidity equilibrium constants showed a significative increase of approximately 1 unit, highlighting the LS role in stabilizing the AH<sup>+</sup> form of C3G.

3.3.2. Determination of LS-C3G Association Constant by UV-visible Spectroscopy. UV-visible spectroscopy was used to assess the interaction of C3G with LS. At all the pH values investigated, a bathochromic shift in the maximum wavelength

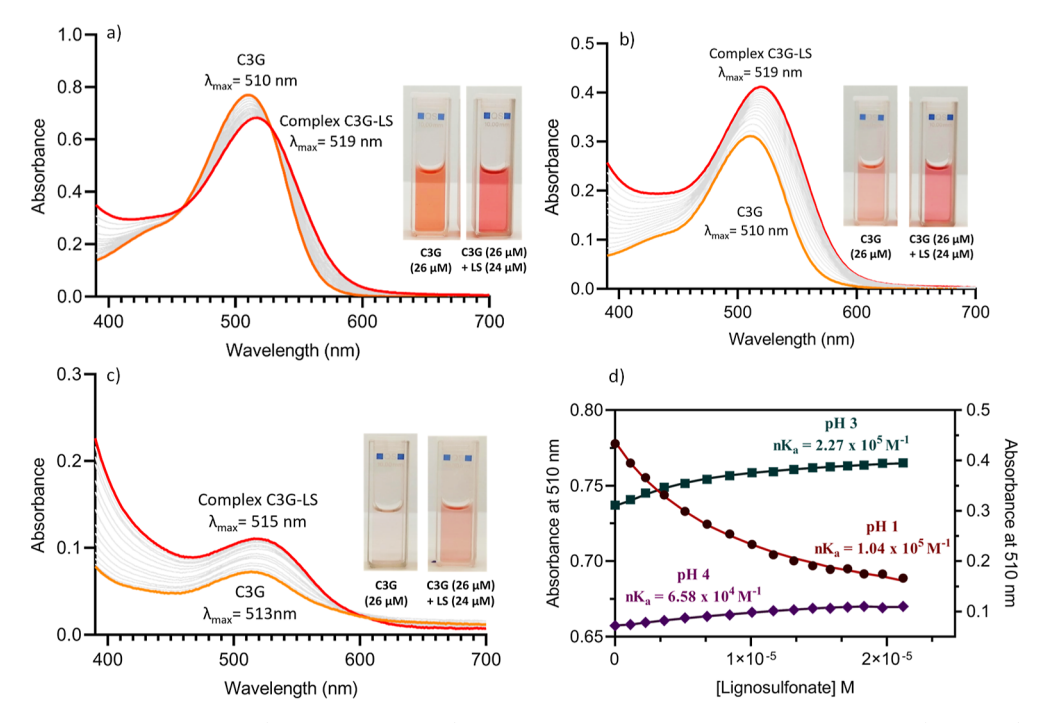


Figure 6. Absorption spectra of free C3G (26  $\mu$ M, orange line) with successive increases in LS concentrations (gray lines) until a maximum concentration of 24  $\mu$ M (red line) at acidic conditions including pH 1 (a), pH 3 (b) and pH 4 (c). The apparent association constants (nK<sub>a</sub>) are determined by fitting the results of the graphic representation of absorbance at 510 nm as a function of LS concentration (d).

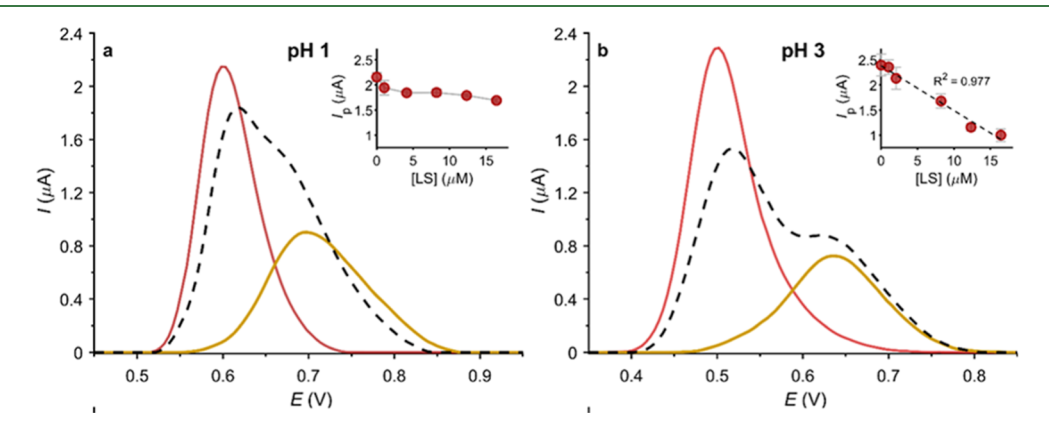


Figure 7. SWVs of 20  $\mu$ M C3G (red trace), 8.2  $\mu$ M LS (yellow trace), and the mixture of the two recorded at pH 1 (a) and pH 3 (b). Insets: Decrease of C3G anodic peak current with increasing concentrations of LS.

of C3G in the presence of LS was observed. A hypochromic effect was also detected with increased LS concentrations at pH 1. This behavior has also been observed with other macromolecules such as dendrimers<sup>46</sup> and curcubit[n]urils.<sup>47</sup> Conversely, at pH 3 (Figures 4 and 6b,c), the bathochromic shift was coupled with an increase in the absorbance intensity for the maximum wavelength (hyperchromic effect). At these pH values, the LS polymer interacts with the flavylium cation and hemiketal present (p $K_h \approx 3.5$ , which means that at pH 3.5 there is 50% of flavylium cation and 50% of other species), shifting the equilibrium toward the formation of more flavylium cation. This suggests that the presence of LS reduces the formation of noncolored species, shifting the equilibrium toward the formation of the flavylium cation, thus preserving the red color. However, the color stabilization was more efficient at pH 3 than pH 4 since the amount of flavylium cation decreased with increasing pH value (10% at pH 4). The complex's apparent association constant  $(nK_2)$  was determined

by the graphical representation of the maximum absorption wavelength as a function of LS concentration (Figure 6d). The results showed a higher binding affinity between LS and C3G at pH 3  $(2.27 \times 10^5 \text{ M}^{-1})$  compared to pH 1  $(1.04 \times 10^5 \text{ M}^{-1})$  $M^{-1}$ ), and pH 4 (6.58  $\times$  10<sup>4</sup>  $M^{-1}$ ). When the number of functional groups in LS (n) available to interact with C3G was included in the mathematical model to calculate the true values of the association constant  $(K_a)$ , the same trend in values and magnitude difference was found for all three pH values (Table S3). Experiments over time demonstrated that at pH 1 the complex forms immediately after LS addition and remains stable since the C3G is only in the chemical form of flavylium cation which interacts with LS. At pH 3, the formation of a stable LS-C3G complex is achieved after 40 min, and in the first 30 min, it was observed a decrease in the absorbance  $(\approx 8\%)$  until it stabilizes (Figure S11); this behavior was associated with the presence of different C3G species in

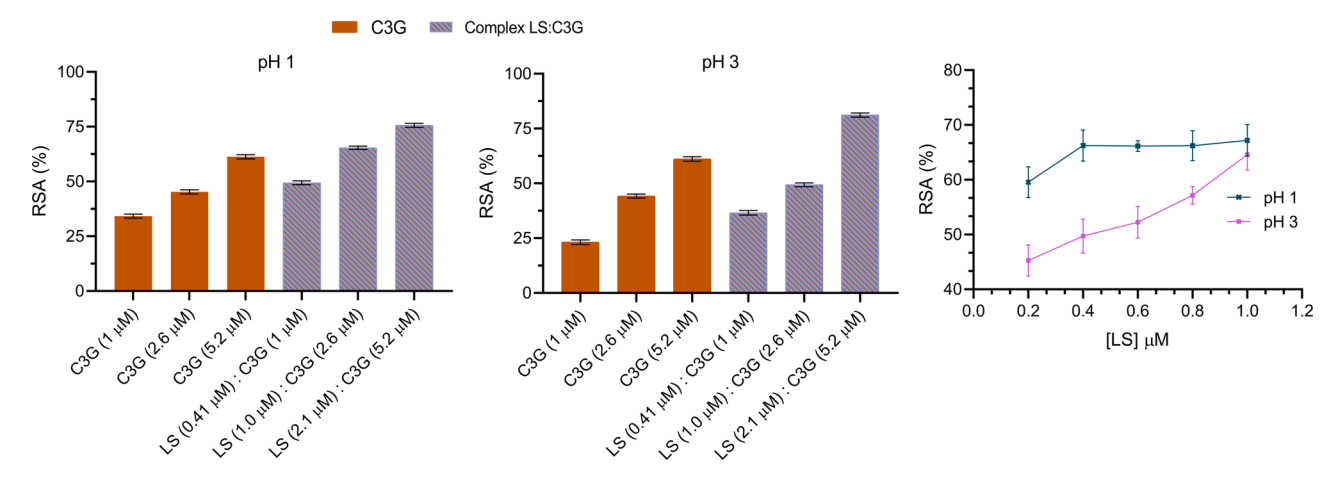


Figure 8. The antioxidant activity of C3G and the complex LS-C3G at pH 1 (a) and 3 (b), for three different concentrations while keeping the anthocyanin-biopolymer ratio constant. Variation of the C3G (2.6  $\mu$ M) antioxidant activity with increasing LS concentrations at both pH.

solution that can interact with LS taking longer time to reach equilibrium.

**3.4.** Oxidative Protection OF C3G Through Voltammetric Response. The stability of ACNs can be compromised in aerobic conditions because these compounds undergo oxidation processes, resulting in the formation of colorless or brown degradation products that reduce the intensity and change the hue of the pigment. Electrochemical studies were conducted to elucidate the redox behavior and interfacial properties of the LS-C3G interactions, and to evaluate possible changes induced by their interaction.

As represented in Figure 7, both LS and C3G showed oxidative processes during the anodic scan (either at pH 1 or pH 3), meaning that they can be oxidized at the working electrode (WE). Due to their polyphenolic nature, LS can be readily (electro)chemically oxidized. The main electroactive subunit is a substituted phenylpropane (C9) group, where methoxyphenol moieties undergo irreversible oxidation to form quinones (Scheme S1).  $^{49,50}$  C3G has two oxidizable centers, the catechol group on ring B being more easily oxidized than the resorcinol group on ring A.  $^{51}$  Consequently, the observed oxidation peak at E = 610 mV (at pH 1) corresponds to the oxidation of the catechol moiety, 3', 4', dihydroxyl groups at ring B to the corresponding o-quinone.  $^{52}$ 

The effect of C3G and LS concentrations on their voltammetric response was traced from 2-100 and 1-20.5  $\mu$ M, respectively (Figure S12). A negative deviation of the anodic peak current response occurred at high concentrations (insets in Figure S12). At pH 3, this effect was also coupled with a positive shift of the peak potential. At both pHs, LS showed a wider and less intense peak compared to C3G, indicating that electron exchange involves an extensive range of oxidizable moieties with a wide distribution of overlapping redox potentials. On the other side, C3G showed higher anodic currents and a lower peak potential, suggesting that it is more prone to oxidation compared to LS. 53 The formation of a poorly electroactive film on the electrode surface occurred for both LS and C3G and was confirmed by the decrease of the anodic currents with consecutive scans (data not shown), demonstrating the importance of the WE cleaning procedure.

SWV was also used to evaluate the reaction and complex formation in the system. The formation of a complex with LS caused a decrease in the anodic peak current of C3G coupled with a positive shift of the peak potential of ca. 10 mV (Figure

7). At pH 1 the presence of LS caused a decrease in the C3G peak current ( $I_{\rm p}$ , -21.5% at the highest LS concentration), without any clear correlation pattern. On the other side, at pH 3 the  $I_{\rm p}$  decreased linearly with LS concentration ( $R^2$  = 0.977) up to -58.2% at the highest LS concentration. This suggests that, at pH 3, LS enhances C3G stability by protecting its oxidizable moieties. Results of LS voltammetric titration by increasing concentrations of C3G (Figure S13) confirm that the interaction mechanism is pH-dependent. The electrochemical stability of the lignosulfonate—cyanidin complex was also investigated for 1 h, showing no modification of successive voltammograms (Figure S14). These results corroborated the formation of a stable complex that protects C3G oxidative stability under standard conditions.

**3.5. Antioxidant Activity.** ACNs are prone to oxidation under certain conditions, such as oxygen exposure, light, and pH changes, which limits their stability in food applications. On the other hand, they are also considered strong antioxidants, able to neutralize reactive oxygen species (ROS) and free radicals, contributing to several health benefits and preventing diseases associated with oxidative stress. Since electrochemical results demonstrated oxidative protection of C3G, the effect on its antioxidant activity was also determined. Figure 8 represents the antioxidant activity expressed in RSA (%) for C3G and the LS-C3G complex at three different concentrations for both pH values. These concentrations were based on the individual behavior of C3G and LS at pH 1 and 3 (Figure S15). The results showed that the LS-C3G complex had higher antioxidant activity than C3G alone (Figure 8a,b). Similar to the oxidative response at pH 3, the RSA of C3G suffered higher modification with the increase of the LS concentration, which increased by 30% between the lowest and highest LS concentrations. For pH 1, the RSA of C3G increased for the first two LS concentrations and remained constant as LS concentrations increased (Figure 8c).

In conclusion, this work demonstrated that the formation of the LS-C3G complex occurs spontaneously and is pH-dependent. At pH 1, the complex forms mainly through electrostatic interactions and hydrogen bonds, while at pH 3, hydrophobic effects coupled with electrostatic interactions are the primary driving forces. The interaction with LS significantly improves two key physicochemical properties of C3G: color and antioxidant capacity. A bathochromic shift in the maximum absorption wavelength of C3G, accompanied by

a significant increase in absorbance intensity at pH 3 and 4, enhances the red color. Additionally, the formation of the LS-C3G complex, particularly at pH 3, reduces the oxidative degradation of C3G, which is a major limiting factor in the application of ACNs.

Improving anthocyanin stability is critical for their use in textiles, cosmetics, and food products. However, it is essential to consider the practical challenges required in scaling up the use of the LS-C3G complex in industrial processes. Lignosulfonates, as byproducts of the paper industry, offer a cost-effective and sustainable solution. On the other hand, factors such as structural heterogeneity, variable reactive group content, impurities, and the presence of sulfur must be considered when using this type of lignin in real-world applications. In cosmetics, lignin is commonly used as a natural antioxidant and UV stabilizer, with a safety profile supported by its nontoxic and biodegradable properties. Regulatory approval in cosmetics is often more flexible, requiring proof of nonirritation and stability. Food-grade lignin must undergo rigorous safety evaluations, including toxicity tests, allergenicity assessments, and compliance with food safety standards set by agencies such as the FDA or EFSA. While lignin holds promise for both industries, its use in food is subject to more stringent oversight to ensure consumer safety.

#### ASSOCIATED CONTENT

# **Supporting Information**

The Supporting Information is available free of charge at https://pubs.acs.org/doi/10.1021/acs.jafc.4c05842.

Details on the PARAFAC modeling used for fluorescence analysis; fluorescence results related to the determination of the linearity for LS at both pH values, 3D fluorescence spectrum at pH 1 for lignosulfonates in the presence of C3G, fluorescence lifetime results for pH 1 and 3, and fluorescence excitation-emission matrix spectra of LS with increasing concentrations of C3G; information on chemical and structural characterization of LS, including the study of the surface charge in aqueous solution; UV-vis spectra for the absorbances of LS and C3G concentrations used for the fluorescence experiments, and the evaluation of the time from the formation of the LS-C3G complex; Square wave voltammograms of the linearity for LS and C3G at both pHs for different concentrations and the titration of lignosulfonates with increasing concentrations of C3G, and time trend of the C3G-LS complex related to the redox stability (PDF)

## AUTHOR INFORMATION

## **Corresponding Authors**

Carlo Bravo – LAQV – REQUIMTE, Departamento de Química e Bioquímica, Faculdade de Ciências, Universidade do Porto, Porto 4169-007, Portugal; ⊚ orcid.org/0000-0002-3805-0404; Email: carlo.bravo@fc.up.pt

Joana Oliveira – LAQV – REQUIMTE, Departamento de Química e Bioquímica, Faculdade de Cîencias, Universidade do Porto, Porto 4169-007, Portugal; ⊙ orcid.org/0000-0002-9996-1463; Email: jsoliveira@fc.up.pt

### **Authors**

Ana Rita Pereira – LAQV – REQUIMTE, Departamento de Química e Bioquímica, Faculdade de Ciências, Universidade

do Porto, Porto 4169-007, Portugal; o orcid.org/0000-0002-9779-2678

Rui Miguel Ramos — LAQV — REQUIMTE, Departamento de Química e Bioquímica, Faculdade de Ciências, Universidade do Porto, Porto 4169-007, Portugal;
orcid.org/0000-0003-0313-6985

Carina Costa – LSRE-LCM – Laboratory of Separation and Reaction Engineering - Laboratory of Catalysis and Materials, Faculty of Engineering, University of Porto, Porto 4200-465, Portugal; ALiCE – Associate Laboratory in Chemical Engineering, Faculty of Engineering, University of Porto, Porto 4200-465, Portugal; orcid.org/0000-0001-5136-3803

Alírio Rodrigues — LSRE-LCM — Laboratory of Separation and Reaction Engineering - Laboratory of Catalysis and Materials, Faculty of Engineering, University of Porto, Porto 4200-465, Portugal; ALiCE — Associate Laboratory in Chemical Engineering, Faculty of Engineering, University of Porto, Porto 4200-465, Portugal; orcid.org/0000-0002-0715-4761

Victor de Freitas – LAQV – REQUIMTE, Departamento de Química e Bioquímica, Faculdade de Ciências, Universidade do Porto, Porto 4169-007, Portugal; orcid.org/0000-0003-0586-2278

Nuno Mateus – LAQV – REQUIMTE, Departamento de Química e Bioquímica, Faculdade de Ciências, Universidade do Porto, Porto 4169-007, Portugal

Ricardo Dias – LAQV – REQUIMTE, Departamento de Química e Bioquímica, Faculdade de Cíências, Universidade do Porto, Porto 4169-007, Portugal

Susana Soares – LAQV – REQUIMTE, Departamento de Química e Bioquímica, Faculdade de Ciências, Universidade do Porto, Porto 4169-007, Portugal; ⊕ orcid.org/0000-0001-8518-9479

Complete contact information is available at: https://pubs.acs.org/10.1021/acs.jafc.4c05842

#### **Author Contributions**

Conceptualization, J.O., C.B., and A.R.P.; methodology, A.R.P, C.B., and S.S.; investigation, A.R.P.; writing—original draft preparation, A.R.P., and C.B.; writing—review and editing, J.O.; C.B.; A.R.; R.R.; C.C.; A.R.; S.S; R.D.; N.M.; V.F.; supervision, J.O., and N.M. project administration, J.O. and N.M. funding acquisition, A.R.; N.M. and V.F. All authors have read and agreed to the published version of the manuscript.

#### Notes

The authors declare no competing financial interest.

# ACKNOWLEDGMENTS

The authors thank Dr<sup>a</sup>. Mariana Ferreira for the use of the fluorimeter. This research was supported by the Associated Laboratory for Sustainable Chemistry, Clean Processes, and Technologies LAQV through the national funds from UIDB/50006/2020 (DOI: 10.54499/UIDB/50006/2020); UIDP/50020/2020 (DOI: 10.54499/UIDP/50020/2020); and ALiCE, LA/P/0045/2020 (DOI: 10.54499/LA/P/0045/2020). A.R.P. gratefully acknowledges her doctoral grant from FCT (SFRH/BD/146549/2019). J.O. would like to thank her contract (2022.00042.CEECIND/CP1724/CT0017).

#### ABBREVIATIONS

LS, lignosulfonates; C3G, cyanidin-3-O-glucoside; ITC, isothermal titration calorimetry; FTIR, Fourier transform infrared spectroscopy; CTAB, hexadecyltrimethylammonium bromide; SWV, square wave voltammograms.

#### REFERENCES

- (1) Santos Buelga, C.; Gonzalez-paramas, A. M. Anthocyanins. In Reference Module in Food Science; Elsevier, 2018; pp 1–12.
- (2) Bridle, P.; Timberlake, C. F. Anthocyanins as natural food colours-selected aspects. *Food Chem.* **1997**, *58* (1–2), 103–109.
- (3) Kong, J.-M.; Chia, L.-S.; Goh, N.-K.; Chia, T.-F.; Brouillard, R. Analysis and biological activities of anthocyanins. *Phytochemistry* **2003**, *64* (5), 923–933.
- (4) Nabi, B. G.; Mukhtar, K.; Ahmed, W.; Manzoor, M. F.; Ranjha, M. M. A. N.; Kieliszek, M.; Bhat, Z. F.; Aadil, R. M. Natural pigments: Anthocyanins, carotenoids, chlorophylls, and betalains as colorants in food products. *Food Biosci.* **2023**, *52*, 102403.
- (5) Pina, F.; Parola, A. J.; Melo, M.; Lima, J. C.; Freitas, V. Chemistry of Anthocyanins. In *Anthocyanins From Natural Sources: Exploiting Targeted Delivery for Improved Health*; Royal Society of Chemistry: UK, 2019; pp 34–76.
- (6) Julia, M.; Eugenia Marta, K.; María José, N.; Agustín, G. A. Antioxidant Capacity of Anthocyanin Pigments. In *Flavonoids*, Goncalo, C. J., Ed.; IntechOpen, 2017.
- (7) Zang, Z.; Tang, S.; Li, Z.; Chou, S.; Shu, C.; Chen, Y.; Chen, W.; Yang, S.; Yang, Y.; Tian, J.; et al. An updated review on the stability of anthocyanins regarding the interaction with food proteins and polysaccharides. *Compr. Rev. Food Sci. Food Saf.* **2022**, 21 (5), 4378–4401.
- (8) Cortez, R.; Luna-Vital, D. A.; Margulis, D.; Gonzalez de Mejia, E. Natural Pigments: Stabilization Methods of Anthocyanins for Food Applications. *Compr. Rev. Food Sci. Food Saf.* **2017**, *16* (1), 180–198.
- (9) Fernandes, A.; Oliveira, J.; Fonseca, F.; Ferreira-da-Silva, F.; Mateus, N.; Vincken, J.-P.; de Freitas, V. Molecular binding between anthocyanins and pectic polysaccharides Unveiling the role of pectic polysaccharides structure. *Food Hydrocolloids* **2020**, 102, 105625.
- (10) Fernandes, A.; Brás, N. F.; Mateus, N.; de Freitas, V. Understanding the Molecular Mechanism of Anthocyanin Binding to Pectin. *Langmuir* **2014**, *30* (28), 8516–8527.
- (11) Fernandes, A.; Brás, N. F.; Oliveira, J.; Mateus, N.; de Freitas, V. Impact of a pectic polysaccharide on oenin copigmentation mechanism. *Food Chem.* **2016**, 209, 17–26.
- (12) Zhao, L.; Pan, F.; Mehmood, A.; Zhang, Y.; Hao, S.; Rehman, A. U.; Li, J.; Wang, C.; Wang, Y. Protective effect and mechanism of action of xanthan gum on the color stability of black rice anthocyanins in model beverage systems. *Int. J. Biol. Macromol.* **2020**, *164*, 3800–3807.
- (13) Chung, C.; Rojanasasithara, T.; Mutilangi, W.; McClements, D. J. Enhancement of colour stability of anthocyanins in model beverages by gum arabic addition. *Food Chem.* **2016**, 201, 14–22.
- (14) He, Z.; Zhu, H.; Xu, M.; Zeng, M.; Qin, F.; Chen, J. Complexation of bovine  $\beta$ -lactoglobulin with malvidin-3-O-glucoside and its effect on the stability of grape skin anthocyanin extracts. *Food Chem.* **2016**, 209, 234–240.
- (15) He, Z.; Xu, M.; Zeng, M.; Qin, F.; Chen, J. Interactions of milk  $\alpha$  and  $\beta$ -casein with malvidin-3-O-glucoside and their effects on the stability of grape skin anthocyanin extracts. *Food Chem.* **2016**, *199*, 314–322.
- (16) Fernandes, A.; Sousa, A.; Azevedo, J.; Mateus, N.; de Freitas, V. Effect of cyclodextrins on the thermodynamic and kinetic properties of cyanidin-3-O-glucoside. *Food Res. Int.* **2013**, *51* (2), 748–755.
- (17) Fernandes, A.; Rocha, M. A. A.; Santos, L. M. N. B. F.; Brás, J.; Oliveira, J.; Mateus, N.; de Freitas, V. Blackberry anthocyanins:  $\beta$ -Cyclodextrin fortification for thermal and gastrointestinal stabilization. *Food Chem.* **2018**, *245*, 426–431.

- (18) Araújo, P.; Basílio, N.; Fernandes, A.; Mateus, N.; de Freitas, V.; Pina, F.; Oliveira, J. Impact of Lignosulfonates on the Thermodynamic and Kinetic Parameters of Malvidin-3-O-glucoside in Aqueous Solutions. *J. Agric. Food Chem.* **2018**, *66* (25), 6382–6387
- (19) Lu, Y.; Lu, Y.-C.; Hu, H.-Q.; Xie, F.-J.; Wei, X.-Y.; Fan, X. Structural Characterization of Lignin and Its Degradation Products with Spectroscopic Methods. *J. Spectrosc.* **2017**, 2017, 1–15.
- (20) Myrvold, B. O. A new model for the structure of lignosulphonates: Part 1. Behaviour in dilute solutions. *Ind. Crops Prod.* **2008**, 27 (2), 214–219.
- (21) Casimiro, F. M.; Costa, C. A. E.; Vega-Aguilar, C.; Rodrigues, A. E. Hardwood and softwood lignins from sulfite liquors: Structural characterization and valorization through depolymerization. *Int. J. Biol. Macromol.* **2022**, *215*, 272–279.
- (22) Li, Q.; Zeng, M.; Zhu, D.; Lou, H.; Pang, Y.; Qiu, K.; Huang, J.; Qiu, X. A Simple and Rapid Method to Determine Sulfonation Degree of Lignosulfonates. *BioEnergy Res.* **2019**, *12* (2), 260–266.
- (23) Lakowicz, J. Principles of Fluorescence Spectroscopy; Springer: New York, 2006.
- (24) Bondet, V.; Brand-Williams, W.; Berset, C. Kinetics and Mechanisms of Antioxidant Activity using the DPPH.Free Radical Method. *LWT* **1997**, 30 (6), 609–615.
- (25) Kontturi, A.-K.; Kontturi, K. Determination of effective charge numbers of polydisperse polyelectrolyte. *J. Colloid Interface Sci.* **1988**, 124 (1), 328–335.
- (26) Kontturi, A. K. Diffusion coefficients and effective charge numbers of lignosulphonate. Influence of temperature. *J. Chem. Soc., Faraday Trans. 1* **1988**, 84 (11), 4043–4047.
- (27) Frazier, R. A.; Papadopoulou, A.; Mueller-Harvey, I.; Kissoon, D.; Green, R. J. Probing Protein—Tannin Interactions by Isothermal Titration Microcalorimetry. *J. Agric. Food Chem.* **2003**, *51* (18), 5189—5195.
- (28) Pina, F. Thermodynamics and kinetics of flavylium salts Malvin revisited. *J. Chem. Soc., Faraday Trans.* **1998**, *94* (15), 2109–2116.
- (29) Leydet, Y.; Gavara, R.; Petrov, V.; Diniz, A. M.; Jorge Parola, A.; Lima, J. C.; Pina, F. The effect of self-aggregation on the determination of the kinetic and thermodynamic constants of the network of chemical reactions in 3-glucoside anthocyanins. *Phytochemistry* **2012**, *83*, 125–135.
- (30) Qian, B. J.; Liu, J. H.; Zhao, S. J.; Cai, J. X.; Jing, P. The effects of gallic/ferulic/caffeic acids on colour intensification and anthocyanin stability. *Food Chem.* **2017**, 228, 526–532.
- (31) Mohamed Ameen, H.; Kunsági-Máté, S.; Bognár, B.; Szente, L.; Poór, M.; Lemli, B. Thermodynamic Characterization of the Interaction between the Antimicrobial Drug Sulfamethazine and Two Selected Cyclodextrins. *Molecules* **2019**, 24 (24), 4565.
- (32) Ross, P. D.; Subramanian, S. Thermodynamics of protein association reactions: forces contributing to stability. *Biochemistry* **1981**, 20 (11), 3096–3102.
- (33) Karimov, O. K.; Teptereva, G. A.; Chetvertneva, I. A.; Movsumzade, E. M.; Karimov, E. K. The structure of lignosulfonates for production of carbon catalyst support. *IOP Conf. Ser. Earth Environ. Sci.* **2021**, 839 (2), 022086.
- (34) Klapiszewski, L.; Jamrozik, A.; Strzemiecka, B.; Matykiewicz, D.; Voelkel, A.; Jesionowski, T. Activation of Magnesium Lignosulfonate and Kraft Lignin: Influence on the Properties of Phenolic Resin-Based Composites for Potential Applications in Abrasive Materials. *Int. J. Mol. Sci.* **2017**, *18*, 1224.
- (35) Shen, Q.; Zhang, T.; Zhu, M.-F. A comparison of the surface properties of lignin and sulfonated lignins by FTIR spectroscopy and wicking technique. *Colloids Surf.*, A **2008**, 320 (1–3), 57–60.
- (36) Djikanović, D.; Kalauzi, A.; Radotić, K.; Lapierre, C.; Jeremić, M. Deconvolution of lignin fluorescence spectra: A contribution to the comparative structural studies of lignins. *Russ. J. Phys. Chem. A* **2007**, *81* (9), 1425–1428.
- (37) Santos, T. J.; Paggiaro, J.; Cabral Silva Pimentel, H. D.; Karla dos Santos Pereira, A.; Cavallini, G. S.; Pereira, D. H. Computational

- study of the interaction of heavy metal ions, Cd(II), Hg(II), and Pb(II) on lignin matrices. J. Mol. Graphics Modell. 2022, 111, 108080.
- (38) Wang, X.; Li, X.; Peng, L.; Han, S.; Hao, C.; Jiang, C.; Wang, H.; Fan, X. Effective removal of heavy metals from water using porous lignin-based adsorbents. *Chemosphere* **2021**, *279*, 130504.
- (39) Yan, M.; Yang, D.; Deng, Y.; Chen, P.; Zhou, H.; Qiu, X. Influence of pH on the behavior of lignosulfonate macromolecules in aqueous solution. *Colloids Surf., A* **2010**, *371* (1–3), 50–58.
- (40) Meng, Y.; Hao, L.; Tan, Y.; Yang, Y.; Liu, L.; Li, C.; Du, P. Noncovalent interaction of cyanidin-3-O-glucoside with whey protein isolate and  $\beta$ -lactoglobulin: Focus on fluorescence quenching and antioxidant properties. *LWT* **2021**, *137*, 110386.
- (41) Ren, C.; Xiong, W.; Li, J.; Li, B. Comparison of binding interactions of cyanidin-3-O-glucoside to  $\beta$ -conglycinin and glycinin using multi-spectroscopic and thermodynamic methods. *Food Hydrocolloids* **2019**, 92, 155–162.
- (42) Ren, S.; Giusti, M. M. Monitoring the Interaction between Thermally Induced Whey Protein and Anthocyanin by Fluorescence Quenching Spectroscopy. *Foods* **2021**, *10* (2), 310.
- (43) Coletta, V.; Rezende, C.; da Conceição, F. R.; Polikarpov, I.; Guimarães, F. E. G. Mapping the lignin distribution in pretreated sugarcane bagasse by confocal and fluorescence lifetime imaging microscopy. *Biotechnol. Biofuels* **2013**, *6*, 43.
- (44) Shen, Q.; Xue, Y.; Zhang, Y.; Li, T.; Yang, T.; Li, S. Effect of microstructure-scale features on lignin fluorescence for preparation of high fluorescence efficiency lignin-based nanomaterials. *Int. J. Biol. Macromol.* **2022**, 202, 520–528.
- (45) Chabbert, B.; Terryn, C.; Herbaut, M.; Vaidya, A.; Habrant, A.; Paës, G.; Donaldson, L. Fluorescence techniques can reveal cell wall organization and predict saccharification in pretreated wood biomass. *Ind. Crops Prod.* **2018**, *123*, 84–92.
- (46) Cruz, L.; Basílio, N.; Mendoza, J.; Mateus, N.; de Freitas, V.; Tawara, M. H.; Correa, J.; Fernandez-Megia, E. Impact of a Water-Soluble Gallic Acid-Based Dendrimer on the Color-Stabilizing Mechanisms of Anthocyanins. *Chem.—Eur. J.* **2019**, 25 (50), 11696–11706.
- (47) Basílio, N.; Pina, F. Flavylium Network of Chemical Reactions in Confined Media: Modulation of 3',4',7-Trihydroxyflavilium Reactions by Host–Guest Interactions with Cucurbit[7]uril. *Chem-PhysChem* **2014**, *15* (11), 2295–2302.
- (48) Arruda, H. S.; Silva, E. K.; Peixoto Araujo, N. M.; Pereira, G. A.; Pastore, G. M.; Marostica Junior, M. R. Anthocyanins Recovered from Agri-Food By-Products Using Innovative Processes: Trends, Challenges, and Perspectives for Their Application in Food Systems. *Molecules* **2021**, *26*, 2632.
- (49) Gawluk, K.; Modrzejwska-Sikorska, A.; Rębiś, T.; Milczarek, G. Preparation of Manganese Lignosulfonate and Its Application as the Precursor of Nanostructured MnOx for Oxidative Electrocatalysis. *Catalysts* **2017**, *7*, 392.
- (50) Milczarek, G. Lignosulfonate-Modified Electrochemical Properties and Electrocatalysis of NADH Oxidation. *Langmuir* **2009**, 25 (17), 10345–10353.
- (51) Cren-Olivé, C.; Hapiot, P.; Pinson, J.; Rolando, C. Free Radical Chemistry of Flavan-3-ols: Determination of Thermodynamic Parameters and of Kinetic Reactivity from Short (ns) to Long (ms) Time Scale. J. Am. Chem. Soc. 2002, 124 (47), 14027–14038.
- (52) Moncada, M. C.; de Mesquita, M. F.; dos Santos, M. M. C. Electrochemical oxidation of the synthetic anthocyanin analogue 4-methyl-7,8-dihydroxyflavylium salt. *J. Electroanal. Chem.* **2009**, *6*36 (1–2), 60–67.
- (53) Novak Jovanović, I.; Miličević, A. A model for the estimation of oxidation potentials of polyphenols. *J. Mol. Liq.* **2017**, 241, 255–259.